Micromechanical Vibratory Rate Gyroscopes Fabricated in Conventional CMOS

Michael S. Kranz* and Gary K. Fedder*†

*Department of Electrical and Computer Engineering and †The Robotics Institute
Carnegie Mellon University
Pittsburgh, PA 15213-3890

Summary

This paper introduces two microelectromechanical vibratory rate gyroscope designs implemented using a conventional CMOS process that uses the metallization and dielectric layers as both electrical interconnect and a microstructural layer. One gyroscope design, the three-fold symmetric gyroscope matches the resonant frequencies of both the driven and the sensed oscillation modes using a highly symmetric suspension. The sensor gain attributable to the device's quality factor is then maximized. A second design, the elastically gimbaled gyroscope, takes advantage of the multiconductor structural layers available in the fabrication process. This design cancels out second-order effects by completely decoupling the drive and sense modes through nesting a proof mass within an outer movable cage. The sensitivity of both designs benefits from the ability to integrate CMOS electronics alongside the mechanical structure.

Introduction

Vibratory-rate surface-micromachined gyroscopes have potential in applications which benefit from a miniature low-cost sensor, such as virtual reality, platform stabilization, and personal navigation. Vibratory-rate gyroscopes use a proof mass suspended by a set of springs and oscillating in some fashion. As shown in Figure 1, a mass is moving with velocity v_x in a stationary frame of reference (x, y). Both the mass and a local frame of reference, (x', y'), are experiencing an external rotation, θ, around the z-axis at a rotational rate, Ω. Since the mass' velocity vector remains constant in the global frame, it appears to rotate in the local frame. That acceleration in the local frame is the Coriolis acceleration, a_c. From that acceleration, a psuedoforce, the Coriolis force, is derived. This force, F_c, acts orthogonal to the velocity in the local frame and is modulated by the external rotation rate. Rotation causes oscillation in an orthogonal mode of the device, which is, in most cases, sensed capacitively.

$$F_c = m\frac{d}{dt}(v_x) = -2mv_x\Omega \tag{1}$$

Bernstein[1] demonstrated a tuning fork gyroscope in which two masses oscillate laterally. An external rotation induces oscillation out of the plane of the device, which is then sensed capacitively. Juneau[2] demonstrated a gyroscope with a rotating mass, where deflections induced by rotations about two axes were also measured out of the plane of the device. Clark[3] described a gyroscope with a single mass oscillating laterally, and with lateral rotation induced deflections sensed capacitively. A gyroscope based on a vibrating ring was demonstrated by Putty[4].

In this paper, we present two new vibratory-rate gyroscope designs which differ in several respects from previous work. In contrast to nonlinear parallel-plate capacitive sensing used in previous designs, our gyroscope topologies use linear sensing elements. The designs also reduce errors and increase sensitivity through the design of the mechanical structure. These devices are fabricated in a novel CMOS process that allows circuitry to be integrated with the microstructure.

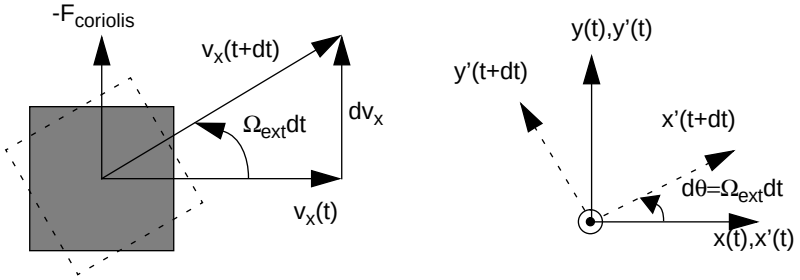

Fig. 1 - For a mass moving with velocity Vx in the global frame of reference (x, y), a local rotating frame of reference (x, y) sees a rotation of the velocity vector, the Coriolis acceleration.

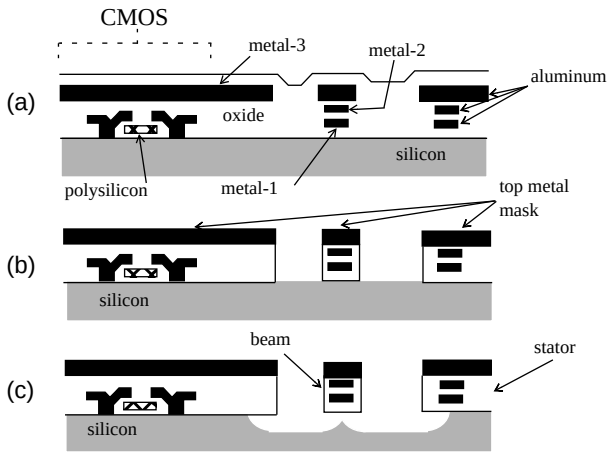

Fig.2 - Cross-sections of process flow. (a) After CMOS processing. (b) After anisotropic oxide etch. (c) After isotropic silicon etch.

Fabrication Process

Mechanical structures are made using the Hewlett-Packard 0.5 μm three-metal n-well CMOS process available through the MOS Implementation Service (MOSIS). To produce a suspended microelectromechanical structure, the metal and dielectric layers combine to form composite structural elements[5]. The top metal layer (metal-3) is used to mask a series of dry etch steps. The microstructural sidewalls are formed by directionally etching the top oxide layers down to the substrate. The mechanical structure is then released from the substrate by isotropically etching the exposed silicon.

The process flow in Figure 2 shows the development of a high-aspect-ratio beam in cross-section. The die which are fabricated through MOSIS have CMOS circuits covered by the metal-3 and oxide layers as shown in Figure 2a. The top metal layer is used as an etch-resistant mask during the subsequent dry etching that creates the composite microstructures. Areas not covered by metal are anisotropically etched in a two step CHF_3/O_2 reactive ion etch (RIE), resulting in the cross-section shown in Figure2b. In Figure 2c, a final SF_6/O_2 low-power isotropic silicon etch releases the structure from the substrate. The dry-etch release prevents breakage and sticking of structures to the substrate and to each other.

This process allows production of beams with a minimum width of 1.5 μm and a maximum width of up to 25 μm. Beams can be comprised of any combination of metal-1, metal-2, or metal-3, and with or without an additional polysilicon layer. A full metal-1, metal-2, and metal-3 beam, composing most of the structures, has a thickness of approximately 5 μm, Young's modulus of 69 GPa, and minimum width of 1.5 μm. Minimum gap widths depend on the amount of masked area surrounding them. It is possible fabricate gaps that are as small as 1.5 μm in width.

An important feature of this process is the ability to fabricate electronic devices adjacent to the mechanical structures to produce a completely integrated microelectromechanical device. The CMOS devices must be inset by at least 30 μm from the side of an etched pit in order to survive the etching processes that releases the mechanical structures. As a result, parasitic capacitances are smaller than those achieved with flip-chip, wire bonding, and other integration processes.

A second key feature of the process is the production of composite structures made up of multiple conductors

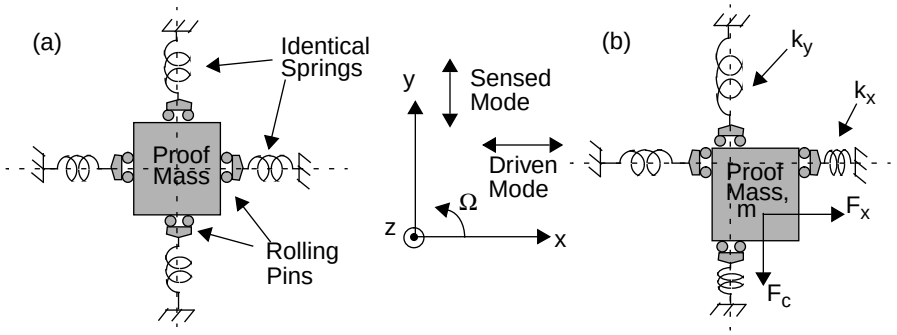

Fig.3 - Schematic diagrams of three-fold symmetric gyroscope, (a) stationary, (b) deflected under forces in x and y

separated by dielectric layers. This allows numerous wiring schemes within a single mechanical structure. The mechanical structures are defined by only one metal layer which remains after the etching process. The other two metal layers and the one polysilicon layer then are available as either additions to the mechanical structure, or as simple interconnect. A suspended mechanical structure need not be constrained at single electric potential. Various parts of the suspended structure, through the use of the metal layers as interconnect, can be placed at different potentials.

Three-Fold Symmetric Gyroscope Design

The three-fold symmetric vibratory-rate gyroscope is shown in schematic in Figure 3a. It consists of a set of identical springs that are placed symmetrically about a central proof mass. These springs are anchored at one end, and connected to the mass at the other end by a rolling pin condition. Deflection of the mass in x and y is depicted in Figure 3b. The rolling pins constrain the springs to act only along the x or y axis. Therefore the restoring forces on the mass are always orthogonal and in line with the x and y axes. The two fundamental modes of oscillation are along the x-axis, the driven mode, and the y-axis, the sensed mode.The mass is forced to oscillate in the driven mode. The Coriolis force induces oscillation in the sensed mode.

The equations of motion (EOM's) for this gyroscope are

$$\ddot{x} = -\omega_x^2 x - \frac{\omega_x}{Q}\dot{x} - F_x + x\Omega^2 + y\dot{\Omega} + 2\Omega\dot{y} - a_x\cos\theta - a_y\sin\theta \tag{2}$$

$$\ddot{y} = -\omega_y^2 y - \frac{\omega_y}{Q}\dot{y} - 2\Omega\dot{x} + y\Omega^2 - x\dot{\Omega} + a_x\sin\theta - a_y\cos\theta \tag{3}$$

$$F_x = F_o\sin(\omega_x t) \tag{4}$$

where $\omega_x^2=k_x/m$, and $\omega_y^2=k_y/m$, are the resonant frequencies of the x and y modes, respectively, a_x and a_y are external accelerations, and Q is the quality factor of resonance. The external acceleration terms can be completely canceled by differential operation of two identical sensors. Force balance of the sensed mode will cancel out any error terms depending on displacement in y. Spring softening terms, the centripetal terms depending on Ω^2, can be canceled through frequency tuning. Terms depending on the rotational acceleration can be digitally canceled using an independent rotational acceleration sensor.

If the forcing function, F_x, is at the resonant frequency of the driven mode, then the displacement of the proof mass is maximized, with a gain of Q, over the static displacement.The frequency of the Coriolis force is then equal to the resonant frequency of the driven mode, with an amplitude modulated by both the maximum displacement of the mass in x and the rate of external rotation.

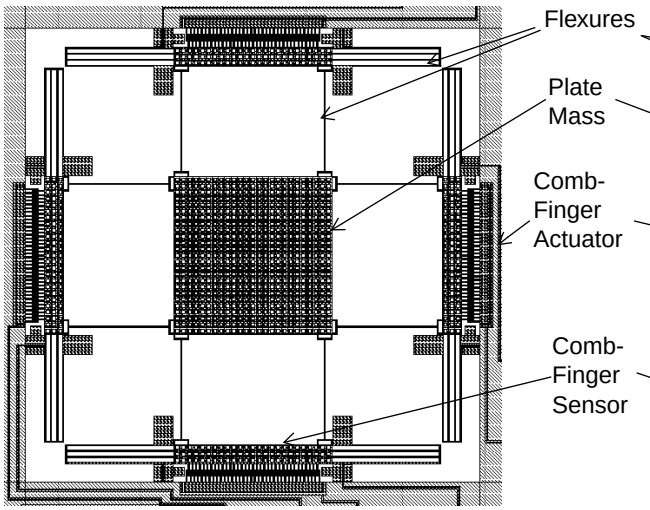

Fig.4 - Three-fold symmetric gyroscope design with the electrostatic drive along the x-axis, and a capacitive displacement sensor along the y-axis.

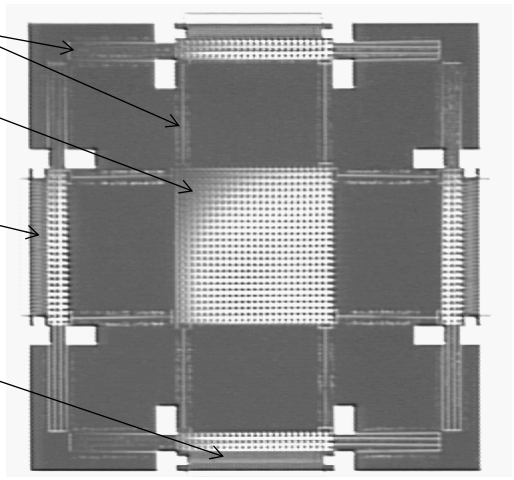

Fig.5 - Optical Micrograph of the Three-Fold SYmmetric Gyroscope fabricated in CMOS.

$$F_c = -2m\Omega\dot{x} = \frac{2m\Omega\omega_x QF_o}{k_x}\cos(\omega_x t) \tag{5}$$

If the resonant frequency of the sensed mode is equal to that of the driven mode, $\omega_x=\omega_y=\omega_r$, then maximum displacement, for a given external rotation rate, will occur in the sensed mode.

$$y = \frac{QF_c}{k_y} = \frac{2m\Omega Q^2\omega_r F_o}{k_x k_y}\cos(\omega_r t) \tag{6}$$

The three-fold symmetric gyroscope inherently matches the resonant frequencies in both oscillation modes by using a completely symmetric suspension, thereby increasing the sensitivity of the device by using the Q-factor to maximize displacements for a given force. The symmetry also reduces effects of process variations on the device sensitivity. In practical implementations of the vibratory-rate gyroscope, the designed Q value is constrained by the necessary bandwidth of the input rotation.

The micromechanical implementation is shown in layout in Figure 4, and the fabricated device is shown in an optical micrograph in Figure 5. The comb-finger actuators apply an electrostatic force in x to the proof mass, exciting the driven mode. When experiencing a constant external rotation, the Coriolis force acts along y and has a frequency equal to that of the excitation frequency. The Q factor of the system provides a gain in the displacement of the sensed mode. The y deflection is sensed with a pair of comb-finger capacitors connected as a differential capacitive voltage divider. A unity-gain buffer detects the divider's voltage and drives off-chip circuitry. This device has a calculated mechanical sensitivity of $6.4*10^{-5}$ μm/deg/sec.

The three-fold symmetric suspension serves two purposes. First, the driven and sensed modes of the device displace different, but identical, spring sets, one set displaces in x and one set displaces in y (see Figure 6, a finite-element simulation of the oscillation modes). Spring constants as well as moving mass are matched along both modes. Therefore, both oscillation modes have equal resonant frequencies. The modes will match even through a uniform process variation, *e.g.*, overetching of the proof mass.

The second purpose of the suspension is to mechanically decouple the x and y deflections of the actuators and

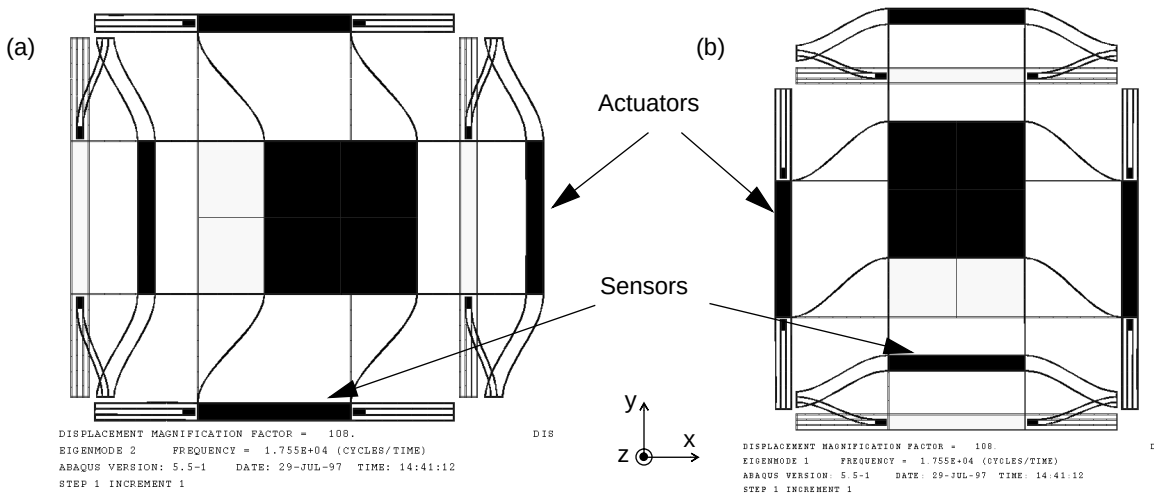

Fig.6 - FEM simulations showing deflection of the mechanical structure in both modes. The grey outline is the undisplaced device, the black outline is the displaced device.(a) Driven x-mode.(b) Sensed y-mode.

sensors. The suspension allows motion of the central mass in both x and y by using complete springs that are very stiff in one direction and very compliant in the other, as an approximation of the rolling pin condition of Figure 3. The masses that attach to the actuators and sensors are placed in the suspension in such a way that they can only move along one axis. So, a deflection of the proof mass in x will not affect the sense mass, which only moves in y. The spring network has reduced the mechanical crosstalk between the sensors and actuators.

There is no experimental data on this device as of yet. Some problems have surfaced with respect to getting the structure released and completely free to move. Some buckling has occurred in the suspension, and a significant amount of curling has taken place. This curling creates problems with the comb-finger structures lining up. Revised designs are currently being fabricated.

Elastically Gimbaled Gyroscope Design

The elastically gimbaled gyroscope is shown in schematic in Figure 7. The design focuses on decoupling the sensed mode from the driven mode by nesting the proof mass and springs within an outer frame, and constraining the motion of the proof mass to the x-axis. The outer frame is then suspended by springs constrained to motion along the y-axis. Mechanical crosstalk is completely eliminated by this design. This reduces errors coupled into the sensor from the driven mode, and allows for independent optimization of the driving and sensing elements.

The device behaves in a manner similar to the previous design. The outer frame is forced to oscillate in the y-direction, the driven mode. When an external rotation is present, the coriolis force induces oscillation of the proof mass in the x-direction, the sensed mode. The deflection of the proof mass with respect to the outer cage is sensed.

The EOM's for this gyroscope are

$$\ddot{y} = -\omega_y^2 y - \frac{\omega_y}{Q}\dot{y} - F_y + y\Omega^2 - m_i\frac{(x\dot{\Omega} + 2\dot{x}\Omega)}{m_i + m_o} + \frac{2m_i + m_o}{m_i + m_o}(a_x\sin\theta - a_y\cos\theta) \tag{7}$$

$$\ddot{x} = -\omega_x^2 x - \frac{\omega_x}{Q}\dot{x} + 2\Omega\dot{y} + x\Omega^2 + y\dot{\Omega} - 2(a_x\cos\theta + a_y\sin\theta) \tag{8}$$

$$F_y = F_o\sin(\omega_y t) \tag{9}$$

As in the previous design, system-based concepts can be applied to cancel out many of these terms. Also, to get a

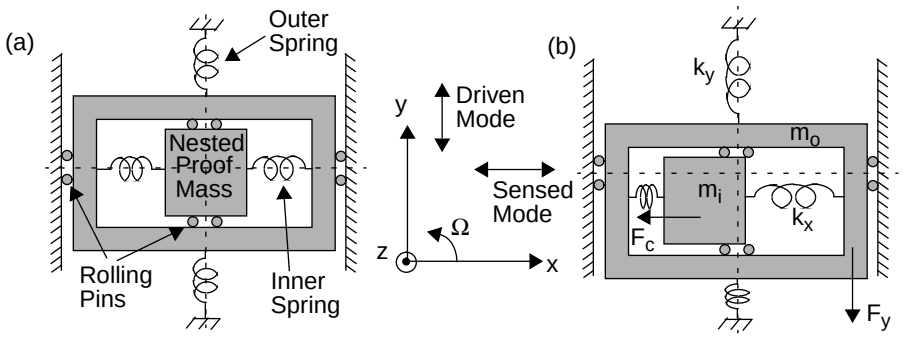

Fig.7 - Schematic view of the elastically gimbaled gyroscope, (a) stationary, (b) under forces in x and y.

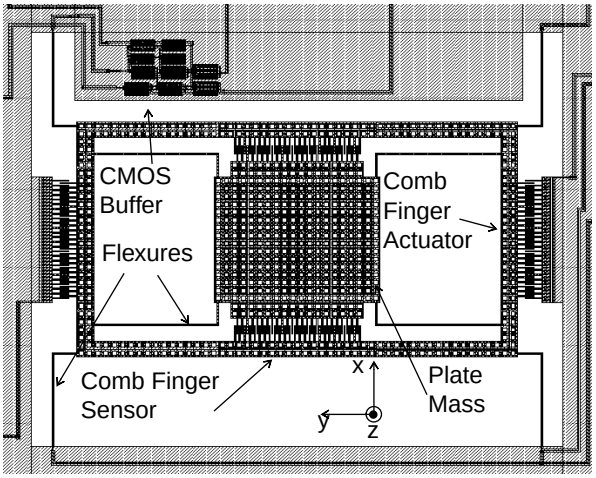

Fig.8 - Elastically gimbaled gyroscope design with the electrostatic drive along the x-axis and capacitive sense of the y displacement.

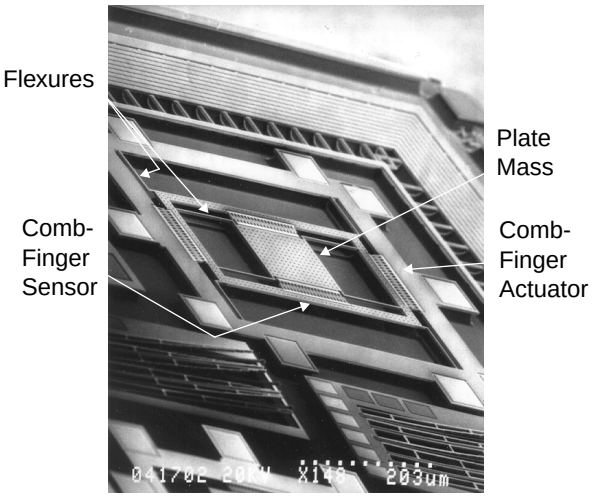

Fig.9 - SEM's of elastically gimbaled gyroscope fabricated in the CMOS process.

gain in the system from Q, the resonant frequencies of each mode are matched by sizing the springs, the outer frame, and the proof mass according to the constraint.

$$\omega_y = \sqrt{\frac{k_y}{m_i + m_o}} = \omega_x = \sqrt{\frac{k_x}{m_i}} \tag{10}$$

A micromechanical implementation of this device is shown in layout in Figure 8, and an SEM of the fabricated device shown in Figure 9. The inner mass is suspended by a flexure to the outer frame. Similarly, the outer frame is attached to the anchors by a separate flexure. Oscillation of the outer frame is induced by a set of electrostatic comb-finger actuators. An external rotation forces the inner mass to move orthogonally with respect to the outer frame. The motion of the inner mass with respect to the outer frame is sensed by a pair of comb-finger capacitive position sensors that move with the outer frame. The position sensors are set up as a capacitive voltage divider and connected to a unity-gain buffer. The calculated mechanical sensitivity for this device is $1.28*10^{-4}$ μm/deg/sec.

The multiconductor features of the CMOS-MEMS fabrication process allow implementation of this gyroscope. The fabrication process does not require that all suspended structures be homogeneously conducting. Hence, the comb-finger structures that sense and induce oscillation can be independently controlled, even though they are on the same suspended mass. Electrical connections to the suspended comb-drive actuators and sensors are made by rout-

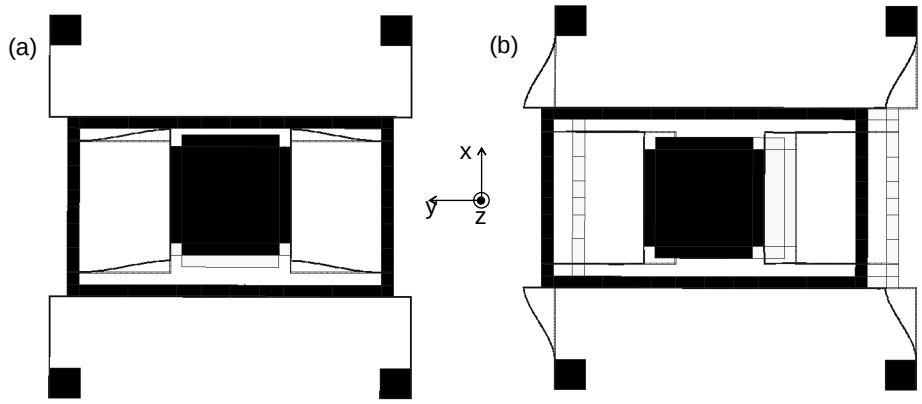

Fig.10 - Finite element simulations showing deflection of mechanical structure under x and y forces. (a) Sensed x-mode. (b) Driven y-mode.

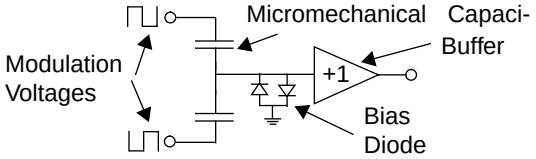

Fig.11 - Gyroscope electrical schematic

ing metal interconnect through the suspensions that mechanically connect the inner mass, outer cage, and anchored frame.

Figure 10 shows a finite-element simulation of the motion of this mechanical structure. Note that the decoupling is degraded by the need to have a non-zero x and y compliance in the suspension to relieve residual stress in the composite-beam microstructural material. Therefore, the suspensions on the inner and outer masses cannot be infinitely stiff in the direction orthogonal to the desired compliant direction. Also, because one mass-spring system is nested within the other, the matching of resonant frequencies to obtain a gain in sensitivity due to the Q factor is more difficult.

The fabricated device has been completely released. The resonant frequency has been measured at 9.9kHz for the driven mode, and 9.8 kHz for the sensed mode. Further testing waits upon the arrival of components necessary to package the device. It is also important to note that curling and residual stress had a smaller impact on this device than it did on the previous device.

Electronics

The fabrication process, since it is a standard CMOS process, allows the integration of sensing electronics within 30 μm of the mechanical structure. A completely integrated sensor can be produced with ultra-low parasitic capacitance values on the high-impedance sense nodes of the device.

The micromechanical capacitors are connected as a capacitive voltage divider. Modulation voltages with an amplitude of 1 V are applied to each end of the divider. At the center of the divider, a buffer circuit senses the voltage (see Figure 11). The buffer circuit is biased at zero volts by the pair of diodes at the input.

The buffer circuit is placed within about 30 μm from the sense nodes of the mechanical device, minimizing par-

asitic capacitances to ground. For this process, the capacitance per unit area of metal-2 (the signal line) to the substrate is 0.0152 fF/μm^2 and to metal-3 is 0.044 fF/μm^2. The gate of the sensing transistor has a capacitance of 3.53 fF/μm^2. For a transistor with minimum width and length (W=0.6 μm, L=0.6 μm) placed 30 μm from the mechanical capacitor and connected by a 1.2μm-wide line, the resulting parasitics total 4.8 fF. In contrast, each mechanical capacitor has a nominal value of 11 fF at zero displacement, with a sensitivity of 1.1fF/μm. With this configuration, the three-fold symmetric gyroscope has a calculated sensitivity of 3.2 μV/deg/sec and the elastically gimbaled gyroscope has a calculated sensitivity of 6.4 μV/deg/sec.

Conclusions

Thin-film vibratory-rate gyroscope mechanisms have been successfully fabricated in an integrated CMOS process. The two designs presented have characteristics which raise sensitivity and cancel undesirable second-order effects. The three-fold symmetric device improves on previous symmetric designs to better match resonant frequencies of the sensed and driven modes to raise sensitivity. Both the three-fold symmetric design, and the elastically gimbaled design are tailored to reduce or eliminate mechanical and electromechanical cross-coupling between the capacitive sensors and electrostatic actuators.

The multiple conductor microstructures available in the CMOS-MEMS process have the flexibility to allow the implementation of novel mechanisms such as the elastically gimbaled gyroscope. These mechanisms may have advantages over polysilicon-based gyroscopes. However, development of a high-aspect-ratio CMOS-MEMS process is ongoing and must be fully characterized in order to design complex structures, such as gyroscopes, successfully. Curling, for example, is a particular problem which we believe can be characterized, and compensated for in designs. Regardless, the integration of the 0.5 um CMOS with MEMS provides a powerful paradigm for future high-performance multi-sensor systems.

Acknowledgment

The authors thank Suresh Santhanam for performing the post-CMOS processing steps and for taking SEM's. Thanks to the staff of the Cleanroom located in the Electrical and Computer Engineering Department and funded in part by the Data Storage Systems Center of Carnegie Mellon University. The research effort was sponsored in part by the Defense Advanced Research Projects Agency under the Air Force Office of Scientific Research, Air Force Materiel Command, USAF, under cooperative agreement F30602-96-2-0304. The U.S. Government is authorized to reproduce and distribute reprints for Governmental purposes notwithstanding any copyright notation thereon. The views and conclusions contained herein are those of the authors and should not be interpreted as necessarily representing the official policies or endorsements, either expressed or implied, of the Air Force Office of Scientific Research or the U.S. Government.

References

[1] J. Bernstein, S.Cho, A.T. King, A. Kourepenis, P. Maciel, and M. Weinberg, "A Micromachined Comb-Drive Tuning Fork Rate Gyroscope," *MEMS'93*, pp. 143-148.

[2] Thor Juneau, A.P. Pisano, James H. Smith, "Dual Axis Operation of a Micromachined Rate Gyroscope," *Transducers'97*, Vol.2, pp.883-886.

[3] William A. Clark, Roger T. Howe, Roberto Horowitz, "Micromachined Z-Axis Vibratory Rate Gyroscope," in the *Technical Digest of the Solid-State Sensor and Actuator Workshop*, Hilton Head, South Carolina, June 2-6, 1996,

pp.283-287.

[4] M. Putty and K. Najafi, "A Micromachined Vibrating Ring Gyroscope," Solid-State Sensors and Actuators Workshop, June13-16, 1994, pp.213-220.

[5] G.K.Fedder, S.Santhanam, M.L.Reed,S.C.Eagle,D.F.Guillou,M.S.Lu, and L.R.Carley, "Laminated high-aspect-ratio structures in a conventional CMOS process," *Sensors and Actuators*, v.A57, no.2, pp. 103-110.

[6] William C. Tang, Tu-Cuong H. Nguyen, Michael W. Judy, and Roger T. Howe, "Electrostatic Comb Drive of Lateral Polysilicon Resonators," *Sensors and Actuators*, A21-A23, 1990, pp. 328-331.